Journal of Veterinary Cardiology (2019) **26**, 39—50

ELSEVIER

Journal of Veterinary Cardiology
ESVC

www.elsevier.com/locate/jvc

Evaluation of non-ECG and ECG-gated computed tomographic angiography for three-dimensional printing of anomalous coronary arteries in dogs with pulmonic stenosis

S.M. Stieger-Vanegas, Dr. med vet, PhD*, K.F. Scollan, DVM, T.W. Riebold, DVM

Department of Clinical Sciences, Carlson College of Veterinary Medicine, Oregon State University, Corvallis, OR, 97331, USA

Received 18 December 2018; received in revised form 25 September 2019; accepted 5 November 2019

KEYWORDS
3D modeling;
R2A;
Fusion deposition modeling;
Canine

Abstract *Introduction/objectives:* Coronary artery abnormalities are described sporadically in dogs, most commonly with pulmonic stenosis. Computed tomographic angiography (CTA) allows non-invasive assessment of coronary anatomy. Three-dimensional (3D) models improve the understanding and visualization of spatially complex anatomy. The study objective was to evaluate coronary artery anomalies using CTA imaging and using rapid prototyping technology to create life-sized coronary artery models of these studies.
Animals, material and methods: Combined retrospective case and prospective pilot study. Inclusion criteria were dogs with reported coronary artery anomalies. The CTA data sets were imported into a medical imaging framework for the analysis of the coronary arteries and into a 3D-planning and printing software for creating printable 3D models. The 3D models were printed using fusion deposition modeling technology.
Results: Six male dogs with an R2A coronary artery anomaly and pulmonic stenosis diagnosed by CTA were included. Electrocardiogram (ECG)-gated CTA allowed better identification of anomalous coronary arteries than non-gated CTA. In all dogs, the right coronary artery had a smaller diameter than the left and the left coronary

Presented in abstract form as a poster presentation at the American College of Veterinary Internal Medicine annual forum 2017, National Harbor, MD, USA.

* Corresponding author.
E-mail address: Susanne.Stieger@oregonstate.edu (S.M. Stieger-Vanegas).

https://doi.org/10.1016/j.jvc.2019.11.004

artery or its branch had a prepulmonic course. All ECG-gated studies were 3D printed while non-gated studies were not printable due to CTA artifacts.
Conclusion: In dogs, CTA is effective for diagnosis of coronary artery anomalies. Printed 3D models of ECG-gated CTA studies were of excellent quality and allowed direct visualization of abnormal coronary artery anatomy. The usefulness of these models to improve the understanding of anomalous coronary artery anatomy could be evaluated in future studies.

Abbreviations

2D	two-dimensional
3D	three-dimensional
CT	computed tomography
CTA	computed tomographic angiography
ECG	electrocardiogram
MDCT	multidetector computed tomography

Introduction/objectives

Congenital or acquired coronary artery abnormalities are infrequently described in dogs. Abnormalities of coronary artery anatomy are most commonly noted in dogs when they occur in combination with pulmonic stenosis. Pulmonic stenosis is one of the most common congenital cardiac diseases in dogs and concurrent coronary artery anomalies have been reported predominately in Boxers and English bulldogs [1—3], although have also been sparsely reported in other breeds including French bulldog, Griffon, American Staffordshire Terrier, Corso, and mixed breed dogs [4,5]. A variety of congenital coronary artery anomalies have been described with the most common in dogs being the R2A anomaly with a single right coronary ostium giving rise to the right coronary artery from which the left coronary artery branches. The course of the left coronary artery is anomalous, located cranial to and encircling the right ventricular outflow tract [1,6]. A single left coronary ostium with a prepulmonic right coronary artery has also been reported in a dog [2]. Balloon valvuloplasty, the recommended therapy for severe pulmonic stenosis, has substantial mortality risk in dogs with any coronary anomaly that includes a prepulmonic course due to the potential of avulsion of the coronary artery and subsequent lethal hemorrhage [7].

Additional rare congenital and acquired coronary artery abnormalities have been reported in dogs [8—10]. Abnormal congenital coronary connections include a right coronary artery to right atrium fistula [11] and a left coronary artery to pulmonary artery shunt [12]. Variations in the path or branching pattern of the coronary arteries have been described, but in the absence of pulmonic stenosis or when no prepulmonic coronary artery course is present, these variations are suspected to be of no clinical significance and may represent inconsequential anatomic variations. Acquired coronary artery disease in dogs appears to be very rare with only a single case report describing an epicardial coronary artery fibromuscular dysplasia causing myocardial infarction and sudden death in a dog [8].

Traditionally, contrast angiography using fluoroscopic guidance, and more recently transesophageal echocardiography [4], have been used in dogs to evaluate the coronary artery anatomy. In dogs and humans, transthoracic echocardiography is considered to be suggestive of but not definitive for coronary artery anomalies [5,13,14]. In human patients, computed tomographic angiography (CTA) is considered the gold standard for the evaluation of the coronary arteries. In dogs, both 16-slice and 64-slice electrocardiogram (ECG)-gated CTA have been shown to be useful in the evaluation of normal and abnormal coronary arteries [15—17]. Additionally, non-ECG-gated 16-slice CTA has been reported to successfully identify coronary artery abnormalities, albeit requiring 4—6 scans per dog to overcome contrast and motion artifacts that limited the ability to assess the anatomy on individual scans [16].

Three-dimensional (3D) printing is a rapidly evolving technology. Although 3D printing of cardiac structures is still in its early stages, especially in veterinary medicine, 3D printed hearts could provide excellent teaching tools for students, residents in training, and veterinarians planning interventional cardiac procedures [18]. Furthermore, these 3D models may help to educate owners to better understand their pet's disease, resulting in a more engaged client participation in the medical decision-making process. Diagnostic

imaging technology has evolved drastically in the last decade and volumetric images can now be reconstructed into 3D image models with relative ease. However, these 3D models are visualized on a two-dimensional (2D) flat screen and thus require the viewer to mentally construct the relationship and proximity of structures as they rotate the image. Printed 3D models have the potential to significantly increase the understanding of complex anatomical structures seen in 2D imaging [19,20].

The aim of this study was to evaluate coronary artery anomalies in dogs using CTA studies and to attempt 3D printing of those studies. We hypothesized that CTA would allow successful evaluation for the presence and anatomic location of anomalous coronary arteries in dogs and allow 3D printing of full-sized models, which will correspond well with the CTA images.

Animals, material and methods

Patient selection

Retrospectively, the medical records of the Lois Bates Veterinary Teaching Hospital at Oregon State University were searched for dogs that had undergone a CTA study between 2009 and 2016. All dogs that were diagnosed with coronary artery anomaly were included in the study. All of the dogs were initially referred for an evaluation of pulmonic stenosis and potential balloon valvuloplasty.

Computed tomographic angiography

All CTA studies were performed with a 64-slice multidetector row computed tomography (MDCT) scanner[a] with the dogs in sternal recumbency. Studies acquired before November 2010 were performed without ECG-gating, and those acquired after that date were performed with ECG-gating due to the acquisition of a MDCT software upgrade and associated hardware. All dogs were anesthetized for the MDCT scans, which was aided by a controlled breath-hold technique during the MDCT scan.

Most dogs ($n = 5$) were sedated with an opioid [butorphanol ($n = 4$), 0.12—0.22 mg/kg IM or 0.05 mg/kg IV; or hydromorphone ($n = 1$)], 0.18 mg/kg IM and a tranquilizer [midazolam ($n = 2$), 0.36—0.45 mg/kg IM] before placement of a venous catheter and induction of anesthesia. One unsedated dog was induced with fentanyl (5 μg/kg), midazolam (0.2 mg/kg), and propofol (3.3 mg/kg) IV. The remaining dogs were induced with midazolam (0.1—0.2 mg/kg IV) and etomidate (0.8—1.1 mg/kg IV), $n = 4$, or propofol (3.9 mg/kg IV), $n = 1$. Anesthesia was maintained with isoflurane following tracheal intubation. Mechanical ventilation ensued with settings intended to cause mild hyperventilation. At the beginning of each MDCT scan, positive end expiratory pressure, 10 cm H_2O, was applied to the airway and the ventilator was paused with the intent to allow the lungs to remain static and slightly distended. After image acquisition, the positive end expiratory pressure was released and mechanical ventilation resumed.

The non-ECG-gated CTA studies were performed with the following parameters: 0.5 mm collimation, 0.5 mm reconstruction interval, a pitch factor of 0.641, gantry rotation speed of 0.4 s, 65—320 mA, and 120 kVp. The retrospective ECG-gated CTA studies were performed with the following parameters: 0.5 mm collimation, 0.5 mm reconstruction interval, a pitch factor of 0.828, gantry rotation speed of 0.35 s, 400—500 mA, and 120 kVp. In all dogs, an unenhanced MDCT scan of the thorax from the thoracic inlet to the most caudal border of the lungs was performed before the non-ECG or ECG-gated contrast-enhanced studies. This unenhanced thoracic MDCT scan was followed by one contrast-enhanced non- or ECG-gated scan of the heart in a cranial to caudal direction, in which the scan length was limited to the heart and ascending aorta and one scan of the entire thorax with the same scan field as the unenhanced MDCT scan. In all dogs, a non-ionic iodinated contrast agent[b] was injected through a peripheral venous catheter using a three-phase injection protocol: 1.5 mL/kg of iodinated contrast agent[b] injected at 3.5 mL/s, followed by 0.5 mL/kg iodinated contrast agent at 2 mL/s, followed by 0.5 mL/kg sterile saline at 2 mL/s. Each dog received a total of 740 mg Iodine/kg bodyweight for the contrast-enhanced computed tomography (CT) scans of the heart and thorax. Automatic bolus tracking with a fixed threshold was used to automatically trigger the cardiac scan when the attenuation of 180 Hounsfield units was detected in a region of interest positioned within the lumen of the proximal descending aorta. In all patients, the region of interest triggered arterial phase scan of the heart was followed by a 60-s

[a] Toshiba America Medical Systems, Inc., Tustin, CA, USA.

[b] Isovue 370, Bracco Diagnostics, Princeton, NJ, USA.

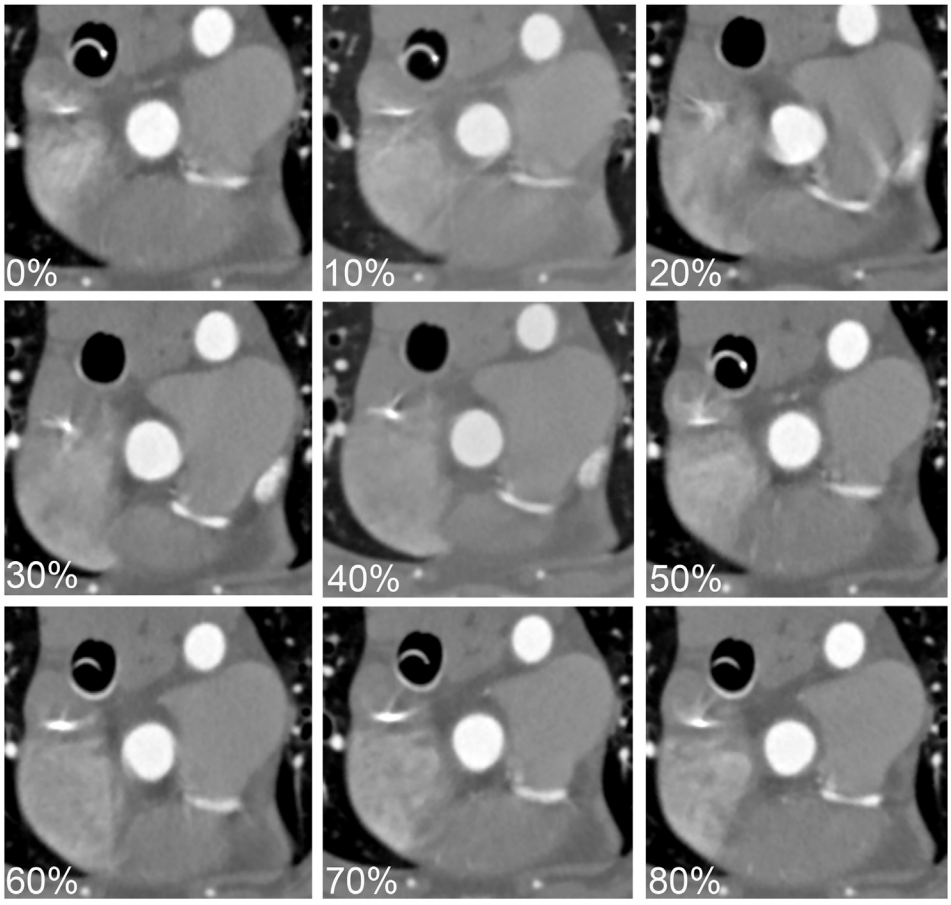

Fig. 1 Transverse computed tomography (CT) images of electrocardiogram (ECG)-gated CT study at different phases of the cardiac cycle (from 0% to 80% R—R interval). The aorta and the left coronary artery, in a prepulmonary course, have varying degrees of motion in each phase of the cardiac cycle. In this dog, the motion is least in the 40%, 70%, and 80% phases of the R—R interval. This is important to evaluate when selecting the reconstruction window.

delayed venous phase non-ECG-gated scan of the entire thorax in all dogs. Following the completion of the study, the patient was weaned off the ventilator, isoflurane administration was discontinued, extubated after it was able to protect its airway, and allowed to recover.

Multiplanar reconstruction of the heart was performed directly on the MDCT scanner to allow for visualization of the heart in standard tomographic views including short- and long-axis one-, two-, and three-chamber views. In addition, oblique reconstructions of the pulmonary artery and aorta or outflow tract at the level of the valves were performed. In all ECG-gated CTA studies, all phases of the cardiac cycle (from 0% to 80% R—R interval) were evaluated and the phase with the least motion to evaluate the coronary artery was selected to create the image reconstructions in standard tomographic views (Fig. 1). All images were sent to a dedicated imaging server for offline analysis and were also transferred to a dedicated workstation with 3D-reconstruction software.[c] Digital Imaging and Communications in Medicine viewer software[d] was used to evaluate all images.

Coronary artery analysis

Initial CTA assessment of the coronary arteries included notation of the origin and path of each coronary artery on 2D images. The number of coronary branches that were able to be identified was recorded in addition to how far distally they could be identified. The diameter of the coronary arteries was measured on the 2D CT images 3—5 mm distal to their origin at the coronary ostium. Additionally, the diameter of the aorta and pulmonary outflow tract was measured in cross-

[c] Vitrea workstation, software version 6.3.2, Vital Image, Inc., Minnetonka, MN, USA.
[d] eFilm, version 3.4, Merge Healthcare, Heartland, WI, USA.

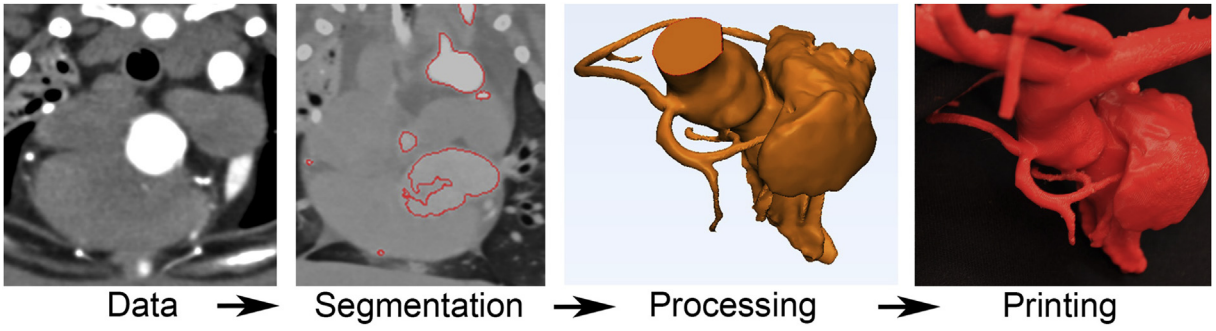

Fig. 2 Outline of the three-dimensional (3D) modeling and printing. First, the computed tomography angiography data set is imported into the 3D-planning and printing software. The areas of interest are segmented and the resulting segmentation mask is processed into a 3D digital model. This 3D model is saved as a stereolithography file, which then can be printed on a 3D printer.

section at the level of the path of the anomalous coronary artery. The CTA data sets were then imported into a medical image-processing framework for 3D analysis of the coronary arteries.[c] Using 3D reconstruction software,[c] a region growing tool with connected threshold criteria was applied on selected areas within the CTA scan to segment the aorta and coronary arteries. The right and left coronary arteries and their branches were visualized, and their anatomic location was described and recorded.

Additionally, the presence of artifacts and the quality of the CTA study for visualizing the coronary arteries were evaluated. The quality of the images assessing coronary artery segments was based on a 3-point scale (0—Poor: significant artifacts present that prohibit the evaluation of the coronary arteries at their origin, 1—Adequate: artifacts are present, but the origins of the coronary arteries can be evaluated, 2—Excellent: minimal artifacts may be present, but the origins of the coronary arteries and distal branches can be evaluated).

Three-dimensional modeling and printing

The CTA data sets were imported into a 3D-planning and printing software[e] (Fig. 2). The vascular volume was segmented, first, on the basis of a threshold intensity in the grey-scale 2D CTA images in various planes (transverse, sagittal, and dorsal). In a second step, the threshold-segmented images were evaluated and if needed a manual segmentation of areas either part or not part of the coronary arteries was performed. This resulted in segmentation masks, which then were converted into a 3D digital model and saved as a stereolithography file (.stl). These stereolithography files were further modified if needed in a computer-aided design software,[e] which allowed adjustment of the 3D model by removing unwanted areas and color-coding the model (Fig. 3).

Following processing, all 3D digital models were assessed for their quality based on a 3-point scale (0—not printable due to lack of visualization of coronary artery origin, 1—coronary arteries visualized; however, artifacts present, 2—excellent quality and coronary arteries visualized, send to printing).

The 3D created models of excellent quality were then printed on a 3D printer.[f] using fusion deposition modeling technology. The 3D models were printed using thermoplastic[g] and water-soluble support materials.[h] The water-soluble support material was then removed in a wave-wash device. All 3D printed models were evaluated for their quality and compared with the CTA studies. Each model was carefully evaluated to assess how many of the distal branches could be printed and if the diameter of the coronary vessels measured using a caliper was similar to the CTA data at the same location previously described.

Results

Six dogs diagnosed with a coronary artery anomaly by CTA were included in the study. All six were male dogs (five intact, one neutered) ranging in age from 4 to 14 months with a median age of 6.5

[e] Materialise, Leuven, Belgium, Europe.

[f] uPrint SE Plus, Stratasys, Eden Prairie MN, USA.
[g] ABSplus™, Stratasys, Eden Prairie, MN, USA.
[h] SR-30XL™ water-soluble support material, Stratasys, Eden Prairie, MN, USA.

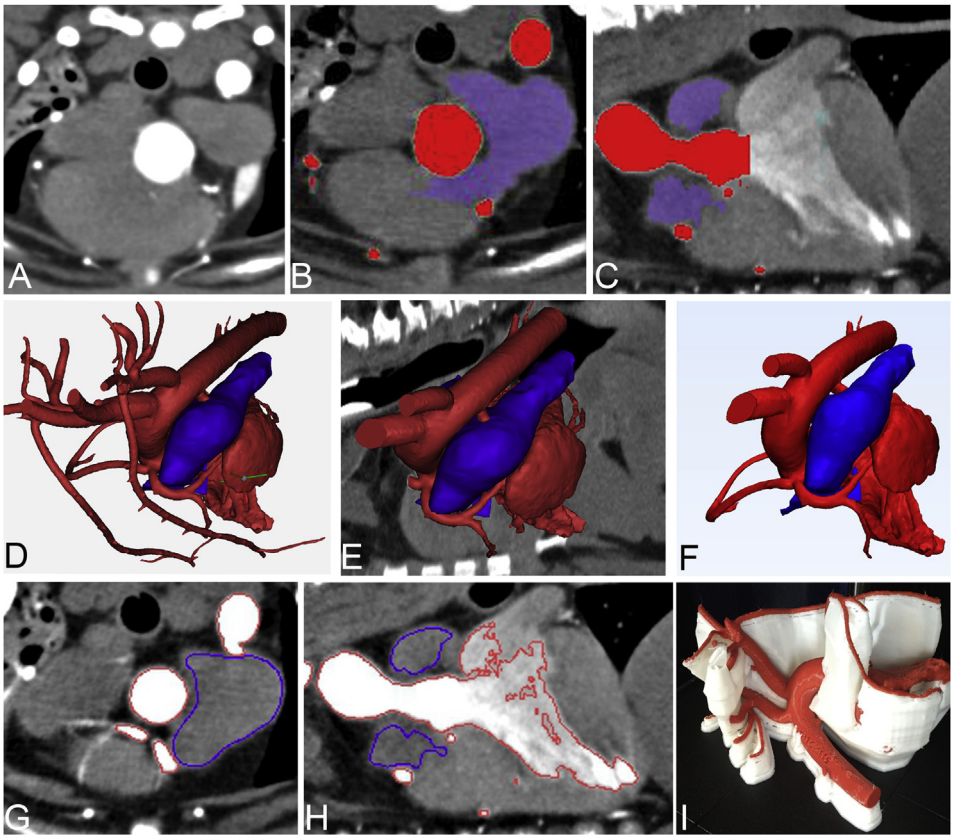

Fig. 3 Process of segmentation and three-dimensional (3D) modeling. (A) The transverse computed tomography (CT) imaging data in 0.5 mm slice thickness are imported into a 3D-planning and printing software. (B) The areas of interested are segmented and stored in a mask. In red, the aorta and its branches and in purple, the pulmonary artery. (C) The segmentation process is performed in various planes, here illustrated in a sagittal image of the heart. (E) From the segmented data set within the mask, a 3D model is calculated. (F) This 3D model can be visualized and superimposed on the CT imaging data. Furthermore, this 3D model can be directly exported as a stereolithographic file for 3D printing. (G) Additionally, the 3D model can be exported into a computer-aided design software and unwanted areas of the model can be removed or other design processes can be performed. (H—I) The computer-aided design software created model can be reimported into the 3D-planning software and be superimposed on the original CT imaging data to evaluate the accuracy of the 3D model. (J) The created stereolithography file of the area of interest can be sent to a 3D printer for printing.

months. Five of the dogs were English Bulldogs and one was a Labrador Retriever mix. The dogs ranged in weight from 8.6 to 21.3 kg with a median weight of 13.8 kg.

Computed tomography angiography findings

All dogs had a single right coronary ostium giving rise to the left coronary artery, which then had a prepulmonary course, termed R2A coronary anomaly, in addition to pulmonic stenosis. In one of the six dogs, the left aortic cusp was smaller than the other two aortic cusps. The right coronary artery was smaller in diameter than the left coronary artery in all dogs with the right coronary ranging in diameter between 25% and 50% of the diameter of the left coronary artery. In three dogs, a short main segment of the left coronary artery was present before it divided into the paraconal interventricular and circumflex ramus. In the remaining three dogs, the left coronary artery immediately branched at the level of the cusp into the left circumflex and interventricular paraconal ramus. In all dogs, the left coronary artery wrapped around the pulmonary outflow tract (Figs. 4A and 5A). In five of six dogs, the diameter of the main pulmonary artery measured in cross-section at the level of the path of the left coronary artery was 25—30% smaller than the diameter of the aorta. In addition to the R2A anomaly, one dog also had an aberrant branching pattern with a small additional vessel extending from the left main coronary artery along the cranial aspect of the aorta dorsally.

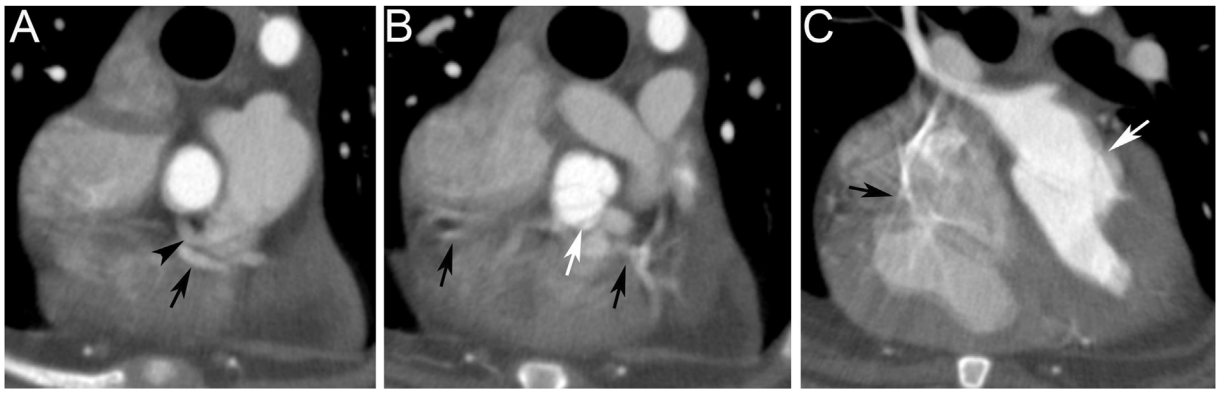

Fig. 4 Cardiac motion and streak artifacts on a non-electrocardiogram (ECG)-gated computed tomography (CT) angiography study. (A) Transverse CT image shows a double image of the left coronary artery (arrow and arrowhead) with a prepulmonary course as noted in a R2A coronary artery anomaly. (B) Transverse CT image of the same dog shows ghosting of the aorta (white arrow) and blurring of the coronary arteries (black arrow). (C) Streak artifact (black arrow) caused by highly attenuating iodinated contrast agent being present in the right atrium in the same dog. Additionally, ghosting of the left ventricle (white arrow) due to cardiac motion is noted.

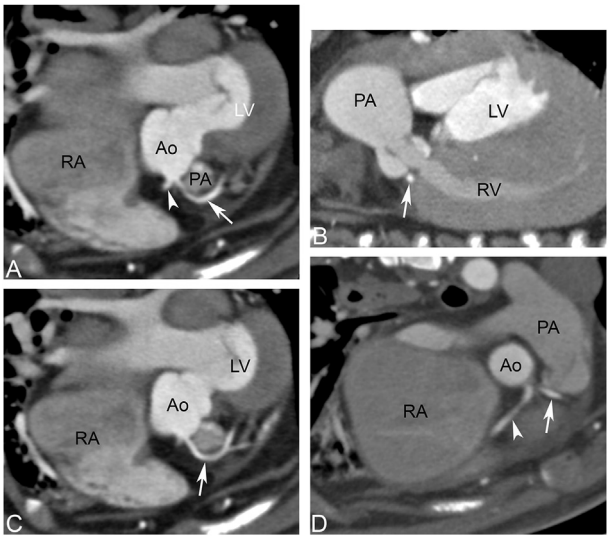

Fig. 5 Electrocardiogram (ECG)-gated study of a dog with an R2A coronary artery anomaly. (A) The right coronary (white arrowhead) and left coronary artery (white arrow) originate from the right cusp of the aorta (Ao). The left coronary artery travels along the cranial aspect of the main pulmonary artery (PA). The pulmonary artery is at this level small as noted by comparing the cross-sectional diameter of the pulmonary artery relative to the aorta. The right atrium (RA) is severely dilated. LV-Left ventricle. (B) On a sagittal image of the heart, the prepulmonary path of the left coronary artery (white arrow) is noted. The pulmonary valve leaflets are thickened and supravalvular stenosis with marked poststenotic dilation of the pulmonary artery (PA) is noted. The right ventricle wall (RV) is severely thickened and similar in thickness when compared to the left ventricle wall. (C) The left coronary artery (white arrow) divides into the left circumflex and interventricular paraconal branch. (D) Severe dilation of the right atrium (RA) is noted. The prepulmonary course of the left coronary artery (white arrow) and the path of the right coronary artery (white arrowhead) is seen.

All dogs had variable degrees of right atrial enlargement and thickening of the right ventricle wall consistent with concentric right ventricular hypertrophy. One dog had a ductus arteriosus, which was contrast filling to the level of the pulmonary artery, but not patent into the pulmonary artery, which is consistent with a ductus diverticulum.

The average heart rate during the cardiac CTA was 120 heartbeats/min [range 96—150 heartbeats/min]; the difference in heart rate in each dog during the cardiac CTA ranged from 0 to 4 heartbeats/minute with an average of 1 heartbeat/min fluctuation. In two dogs, the Labrador Retriever mixed breed dog (non-ECG-gated) and one English bulldog (ECG-gated), the heart rate was at or above 140 heartbeats/minute.

Non-gated CTAs were performed in two of six and ECG-gated studies were performed in the other four dogs. The quality of visualizing the coronary arteries was assessed in both non-gated CTA studies as a 1, meaning that the coronary arteries and their anomalous path could be visualized, but motion artifacts were present. Both non-ECG-gated CTA had cardiac motion-related artifacts resulting in image blurring, winging, stair stepping, and double images of the coronary arteries, but allowed visualization of the coronary artery anomaly (Fig. 4). Additionally, variable degrees of beam-hardening artifacts were noted in the CTA scans. In all non-ECG-gated CTA studies, the left coronary artery was depicted as a double image (Fig. 4A) and evaluation of the distal branching pattern of the coronary arteries was limited or could not be performed due to the presence of motion-related artifacts.

The quality of visualizing the coronary arteries in all ECG-gated CTA studies was recorded as a 2, demonstrating that all studies were of excellent quality allowing visualization of the coronary arteries and their distal branching patterns (Fig. 5).

Three-dimensional modeling and printing findings

The creation of 3D models from non-ECG-gated CTA studies was challenging due to the misregistration of slices and motion artifact, resulting in blurred or doubled segmented vessels. Extensive manual segmentation was attempted to identify and delineate the coronary arteries but did not result in a printable quality stereolithography file. Neither of the non-ECG-gated CTAs was of a quality to be printed as 3D models and therefore each had a modeling score of 0.

On ECG-gated CTA studies, segmentation of the right and left coronary arteries, left circumflex and interventricular coronary arteries, as well as the origin of the smaller branches supporting the left atrial, left ventricular, and right ventricular walls were easily segmented. However, the segmentation of the more distal branches was challenging due to their small size. The branches were visualized containing luminal contrast agents but could only be segmented manually. The Hounsfield units measured in these small coronary artery branches were less than 200 and these smaller

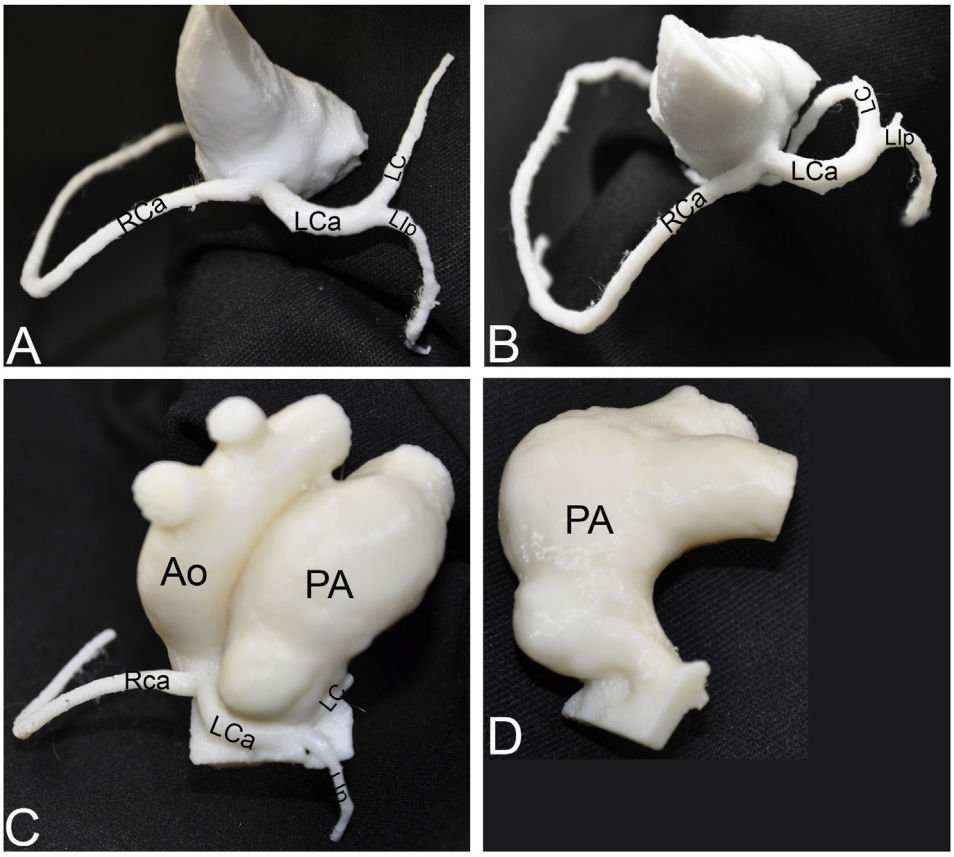

Fig. 6 Various printed (three-dimensional) 3D models of the aortic root of three dogs (dog 1 = A, dog 2 = B, dog 3 = C—D) with a R2A coronary anomaly as noted by a single origin of the right coronary artery (RCa) and left coronary artery (LCa) and a prepulmonary course of the left coronary artery. (A) This dog was the only case in this study, where the left coronary artery had a wider path around the main pulmonary artery with the main pulmonary artery being about 2—3% smaller in diameter compared to the aorta at the level of the left coronary artery. (B) In this dog, the left coronary artery extends in a narrow circle around the main pulmonary artery (not shown). The left coronary artery divides on the left lateral aspect of the pulmonary artery into the left circumflex (LC) and paraconal interventricular (LIp) branches. The left circumflex branch gives off a proximal left atrial branch, which winds in an aberrant path around the main pulmonary artery extending along the cranial border of the aorta ventrally and towards the left atrium (C—D) In this dog, similar to the dog in B, the left coronary and its paraconal branch (LC) encircles the main pulmonary artery (PA). The left coronary artery divides at a similar level into the left circumflex and paraconal branches (LIp).

branches measured less than 1.7 mm in diameter. Using a semiautomated technique to segment the vessels reduced time during the segmentation process, but the additional manual segmentation needed for smaller branched resulted in a more time-consuming process. Manual segmentation was often needed when the vessel diameter was very small and when the contrast enhancement in the vessel was low. The 3D models created from the four ECG-gated CTA studies could and were all printed (Fig. 6) and therefore each had a modeling score of 2.

Discussion

In the study presented here, all CTA scans, including non-gated and ECG-gated MDCT scans, were diagnostic for visualizing the coronary arteries and identifying anomalous anatomy. However, motion artifacts and blurring present on non-ECG-gated CT scans resulted in more difficulty assessing the coronary anatomy and could create the potential to misinterpret normal or abnormal vessels, especially when coronary artery anomalies other than R2A anomaly may be present. Our results are concordant with previously published veterinary studies that reported the use of ECG-gated [15] and non-ECG-gated [16] CTA to diagnose abnormal coronary artery anatomy in dogs. Based on the findings of these studies and our results, the use of ECG-gating offers the advantages of requiring fewer scans per dog to provide a diagnosis, which reduces radiation exposure to the patient, having fewer image artifacts, and allowing the evaluation of the distal branches of the coronary arteries. Additionally, in our study, only ECG-gated MDCT scans provided images that allowed the creation of accurate 3D printed models while non-ECG-gated images were not printable due to substantial image artifacts.

The coronary arteries are relatively small vessels that undergo movement within the chest cavity associated with myocardial motion during the cardiac cycle. Because of these inherent challenges, the ideal imaging modality to assess the coronary arteries would have high spatial and temporal resolution. The development of multidetectors, slip-ring technology, and faster gantry rotation speeds has dramatically increased the temporal resolution of CT scanners. For these reasons, MDCT scans are now commonly used to assess the coronary arteries in humans [21] as a non-invasive alternative to selective fluoroscopic angiography. Electrocardiogram-gating technology links the CT scanner to the patient's cardiac rhythm and allows continuous scanning with retrospective gating that delineates images from specific cardiac cycle time points, or prospective gating in which the scanner only acquires images during specific portions of the cardiac cycle. In our study, we performed retrospective ECG-gating as it provided the opportunity to retrospectively modify which aspects of the CTA were used for creating the images by removing sections where the heart rate is irregular. For ideal ECG-gated scans of the coronary arteries, the patient's respiratory motion should be minimized by a breath hold, as we attempted in our study, and the heart rhythm should be regular.

The two most common artifacts noted in our CTA studies were stairstep and motion artifacts. Stairstep artifacts are usually caused by an irregular heart rhythm resulting in misregistration of the image data. Motion artifacts caused by respiratory or cardiac movement can cause image blurring, winging, stair stepping, or a double image of the coronary arteries. Motion artifacts in our study were mainly caused by cardiac motion as all dogs were scanned under general anesthesia and the respiratory motion was controlled with a breath-hold technique. We found heart rate regularity and rate stability to be critical in reducing artifacts with retrospective ECG-gating. In our experience, cardiac motion artifacts, despite ECG gating, are frequently caused by tachycardia or by variability in the beat-to-beat intervals during the image acquisition, which is similarly also reported as a common artifact seen in human cardiac studies [22]. With our MDCT unit, a heart rate range for scanning is established by the ECG-gating software prior to the start of scanning and contrast administration. Artifacts may occur if the patient's heart rate is not stable and gradually increases or decreases out of the predetermined range once scanning has begun resulting in a stair-step artifact or no images created of some part of the heart.

Additionally, in some of our studies, beam-hardening artifacts that can be due to highly attenuating objects such as bone, metal, or iodinated contrast agents within the x-ray beam were present. As the beam-hardening artifacts in our study were predominately noted at the cranial aspect and right side of the heart, we hypothesize that they were likely caused by a portion of the contrast agent bolus persistently present in the cranial vena cava or right atrium and this resulted in hypoattenuating streaks through the ascending aorta. Despite these beam-hardening artifacts, the coronary artery origin and prepulmonary path of

the left coronary artery could consistently be evaluated.

Some of these common artifacts can be avoided or reduced by patient preparation and post-processing of the images. In ECG-gated CTA studies, cardiac motion can be reduced by reconstructing the images of the heart during the diastolic phase of the R—R interval, when minimal cardiac motion is present. Additionally, our ECG-gating software allows for manual postprocessing of the R—R intervals, therefore irregular R—R intervals can be excluded from the reconstructions. We did not utilize prospective ECG-gating for our CTA scans, although this technique is commonly used in humans since the acquisition of only diastolic CTA images yields relatively motionless images while reducing radiation exposure to the patient [23]. In our two CTA studies performed without ECG-gating, no postprocessing correction mechanisms were available and therefore artifacts that hindered evaluation could not be rectified.

It is reported that when ECG-gating is not available for a CT scan, slowing the heart rate with oral or parenteral medications, most frequently β-blockers, will decrease the motion velocity of the coronary arteries and increase the relative and absolute duration of the diastole in the cardiac cycle. This should reduce image blurring secondary to cardiac motion. Unfortunately, in a previous canine study, the use of esmolol during CTA scans did not result in reaching the target heart rate of 60—65 beats/min [17]. In humans, heart rates less than 60 beats/min have been proposed as ideal for coronary CT imaging and higher heart rates have been shown to reduce image quality [24,25]. The ideal heart rate for coronary CT imaging in dogs is unknown, although based on the use of similar CT scanners in veterinary centers to human centers, the rate of 60—80 beats/min would represent a reasonable target to minimize motion artifact; however, in our study the heart rate of our dogs was higher. In our experience, the regularity of the beat-to-beat interval has been more important than the absolute heart rate with respect to minimizing artifacts with retrospective ECG-gating. In our study, the heart rate fluctuated minimally with a maximum of 4 heartbeats/min increase during the cardiac CTA.

Beam-hardening artifacts may have been reduced by making modifications to the contrast agent injection protocol. We have implemented a saline flush for our cardiac studies, which helps to reduce streaking, caused by contrast agents remaining in the cranial vena cava. At our institution, the intravenous catheter for contrast agent injection is commonly placed in the front limbs or neck; however, placement of the intravenous catheter in the hind limbs is potentially more favorable when imaging the coronary arteries is performed, as the contrast agent within the caudal vena cava would not result in beam-hardening artifacts of the ascending aorta and therefore likely reduce the degree of streaking in the area of interest. Using a large bore catheter allows higher contrast agent injection rates and reduces the injection duration resulting in less contrast agent still present in the cranial vena cava and right side of the heart during the CT scan. Additionally, the tube current could be increased to reduce streaking; however, this would result in a higher patient exposure.

The larger size of the left coronary artery compared to the right coronary artery in all six dogs included in our study is consistent with the reported normal anatomy of the right coronary artery and left dominance of the coronary artery system in the dog [16,26,27]. The R2A coronary anomaly was the main abnormality noted in our study, which is consistent with published literature reporting the R2A coronary abnormality as the most common coronary artery abnormality observed in dogs [1,4].

At this time, there is little experience using rapid printing technology in veterinary cardiology. Our study demonstrated that with currently available CT technology, precise models of anomalous coronary arteries in dogs can be fabricated. These models allowed evaluation of the relationship between the coronary arteries and the pulmonary outflow tract. The herein presented experience with 3D modeling demonstrates that in dogs it is feasible to print vascular structures less than 1.7 mm in diameter. In all our studies, a combination of automated and manual segmentation was used; however, with ECG-gated studies, the manual segmentation was only needed for the more distal and smaller sized coronary branches where the minimal amount of luminal contrast agent present was not detected by the automated segmentation process.

The advantageous applications of 3D printed models of cardiac and vasculature structures are currently being explored in medical education, surgical, and interventional planning. The ability to print 3D models of coronary anatomy and complex congenital defects provides a tremendous educational resource to facilitate training veterinary students, residents, and clients. The ability to manipulate these 3D models should aid the evaluation and comprehension of the spatially complex anatomy and therefore provide a better

understanding of the morphometry of the disease process. Currently, the authors utilize one of these printed models in the hospital exam room to demonstrate the 3D anatomy of the R2A anomaly to clients. Three-dimensional printing has provided a tool to augment preprocedural planning and training in various fields [28] and in some cases the fabrication of patient-specific interventional devices [29].

Three-dimensional printing has been used to create vascular flow models and simulation models for training interventional catheterization skills. Three-dimensional modeling of the vascular structures in dogs with pulmonic stenosis with coronary vascular anomalies might be useful in creating vascular flow models that would allow assessment of potential interventional procedures in phantoms before being performed in an actual patient. The use of simulation models in materials with similar properties to actual tissue might improve the haptic experience and improve interventional procedural skills while reducing patient risks.

Rapid fabrication is still a relatively new technology, especially in veterinary medicine and presents a range of new challenges. Currently, the most prominent issues and challenges associated with 3D printing are the time commitment required for segmentation and fabrication and the costs of 3D printers and fabrication materials. These challenges may be overcome with improvements in segmentation software, CT scan settings optimized prospectively for 3D printing, and operator familiarity and skill.

Our study had several limitations, including the small number of CT scans of anomalous coronary vessels available for evaluation. Furthermore, we were not able to evaluate the impact of 3D printed coronary artery models on the clinician, student, or client understanding due to the retrospective nature of the images utilized.

Conclusions

Our study illustrates that non-ECG-gated MDCT is sufficient to demonstrate an R2A coronary anomaly in dogs, however, ECG-gated images are of better quality and allow a more accurate and detailed evaluation of coronary arteries. Furthermore, ECG-gated CTA data allowed 3D printed coronary artery models to be created while non-gated CTA studies contained artifacts that precluded 3D printing. Additionally, our study provides proof of concept for the feasibility of fabricating small-sized vessels such as anomalous coronary arteries of dogs with pulmonic stenosis using fusion deposition modeling technology. Printed 3D coronary artery replicas can illustrate the relationship of the coronary arteries with adjacent cardiac anatomic structures, especially the pulmonic valve and pulmonary artery. This could provide students, veterinarians in training, and clients with an improved understanding of the anatomic relationship between these structures, especially in patients in which a balloon valvuloplasty is planned.

Conflict of Interest Statement

The authors report no financial or other conflicts related to this report.

Acknowledgements

This study was in part supported by a College of Veterinary Medicine summer research grant and the Camden endowment. We thank Rachel Cunningham for assistance in data collection.

References

[1] Buchanan JW. Pulmonic stenosis caused by single coronary artery in dogs: four cases (1965—1984). J Am Vet Med Assoc 1990;196:115—20.
[2] Visser LC, Scansen BA, Schober KE. Single left coronary ostium and an anomalous prepulmonic right coronary artery in 2 dogs with congenital pulmonary valve stenosis. J Vet Cardiol 2013;15:161—9.
[3] Waterman MI, Abbott JA. Novel coronary artery anomaly in an English Bulldog with pulmonic stenosis. J Vet Intern Med 2013;27:1256—9.
[4] Navalon I, Pradelli D, Bussadori CM. Transesophageal echocardiography to diagnose anomalous right coronary artery type R2A in dogs. J Vet Cardiol 2015;17:262—70.
[5] Scansen BA. Coronary artery anomalies in animals. Vet Sci 2017;4.
[6] Buchanan JW. Pathogenesis of single right coronary artery and pulmonic stenosis in English Bulldogs. J Vet Intern Med 2001;15:101—4.
[7] Kittleson M, Thomas W, Loyer C, Kienle R. Single coronary artery (type R2A). J Vet Intern Med 1992;6:250—1.
[8] Mete A, McDonough SP. Epicardial coronary artery fibromuscular dysplasia, myocardial infarction and sudden death in a dog. J Comp Pathol 2011;144:78—81.
[9] Turk MA, Turk JR, Hopkins MG, Wagner JA. Unexpected death in an adult dog with anomalous origin of the left coronary artery from the pulmonary trunk. Cornell Vet 1984;74:344—8.
[10] Tangkawattana P, Muto M, Nakayama T, Karkoura A, Yamano S, Yamaguchi M. Prevalence, vasculature, and innervation of myocardial bridges in dogs. Am J Vet Res 1997;58:1209—15.

[11] Jacobs GJ, Calvert CA, Hall DG, Kraus M. Diagnosis of right coronary artery to right atrial fistula in a dog using two-dimensional echocardiography. J Small Anim Pract 1996; 37:387—90.
[12] Pelosi A, Cote E, Eyster GE. Congenital coronary-pulmonary arterial shunt in a German shepherd dog: diagnosis and surgical correction. J Vet Cardiol 2011;13: 153—8.
[13] Angelini P. Is echocardiography adequate to identify the severity of anomalous coronary arteries? JACC Cardiovasc Imaging 2016;9:898—9.
[14] Gunther-Harrington CT, Phillips KL, Visser LC, Fousse SL, Stern JA. Non-electrocardiographic-gated computed tomographic angiography can be used to diagnose coronary artery anomalies in Bulldogs with pulmonary valve stenosis. Vet Radiol Ultrasound 2019;60:38—46.
[15] Drees R, Johnson RA, Pinkerton M, Del Rio AM, Saunders JH, Francois CJ. Effects of two different anesthetic protocols on 64-MDCT coronary angiography in dogs. Vet Radiol Ultrasound 2015;56:46—54.
[16] Auriemma E, Armienti F, Morabito S, Specchi S, Rondelli V, Domenech O, Guglielmini C, Lacava G, Zini E, Khouri T. Electrocardiogram-gated 16-multidetector computed tomographic angiography of the coronary arteries in dogs. Vet Rec 2018;183:473.
[17] Drees R, Frydrychowicz A, Reeder SB, Pinkerton ME, Johnson R. 64-multidetector computed tomographic angiography of the canine coronary arteries. Vet Radiol Ultrasound 2011;52:507—15.
[18] Dundie A, Hayes G, Scrivani P, Campoy L, Fletcher D, Ash K, Oxford E, Moise NS. Use of 3D printer technology to facilitate surgical correction of a complex vascular anomaly with esophageal entrapment in a dog. J Vet Cardiol 2017;19:196—204.
[19] Matsumoto JS, Morris JM, Foley TA, Williamson EE, Leng S, McGee KP, Kuhlmann JL, Nesberg LE, Vrtiska TJ. Three-dimensional physical modeling: applications and experience at Mayo Clinic. RadioGraphics 2015;35:1989—2006.
[20] Preece D, Williams SB, Lam R, Weller R. "Let's get physical": advantages of a physical model over 3D computer models and textbooks in learning imaging anatomy. Anat Sci Educ 2013;6:216—24.
[21] Tabari A, Lo Gullo R, Murugan V, Otrakji A, Digumarthy S, Kalra M. Recent advances in computed tomographic technology: cardiopulmonary imaging applications. J Thorac Imaging 2017;32:89—100.
[22] Kalisz K, Buethe J, Saboo SS, Abbara S, Halliburton S, Rajiah P. Artifacts at cardiac CT: physics and solutions. RadioGraphics 2016;36:2064—83.
[23] Sun Z, Ng KH. Diagnostic value of coronary CT angiography with prospective ECG-gating in the diagnosis of coronary artery disease: a systematic review and meta-analysis. Int J Cardiovasc Imaging 2012;28:2109—19.
[24] Dewey M, Vavere AL, Arbab-Zadeh A, Miller JM, Sara L, Cox C, Gottlieb I, Yoshioka K, Paul N, Hoe J, de Roos A, Lardo AC, Lima JA, Clouse ME. Patient characteristics as predictors of image quality and diagnostic accuracy of MDCT compared with conventional coronary angiography for detecting coronary artery stenoses: CORE-64 Multicenter International Trial. AJR Am J Roentgenol 2010;194: 93—102.
[25] Mahabadi AA, Achenbach S, Burgstahler C, Dill T, Fischbach R, Knez A, Moshage W, Richartz BM, Ropers D, Schroder S, Silber S, Mohlenkamp S. Safety, efficacy, and indications of beta-adrenergic receptor blockade to reduce heart rate prior to coronary CT angiography. Radiology 2010;257:614—23.
[26] Evans HE, Christensen GC, Miller ME. In: Evans HE, Christensen GC, editors. Miller's anatomy of the dog. 2nd ed. Philadelphia: Saunders; 1979.
[27] Oliveira CL, David GS, Carvalho MD, Dornelas D, Araújo S, da Silva NC, Ruiz CR, Fernandes JR, Wafae N. Anatomical indicators of dominance between the coronary arteries of dogs. Int J Morphol 2011;29:845—9.
[28] Saunders AB, Keefe L, Birch SA, Wierzbicki MA, Maitland DJ. Perceptions of transcatheter device closure of patent ductus arteriosus in veterinary cardiology and evaluation of a canine model to simulate device placement: a preliminary study. J Vet Cardiol 2017;19: 268—75.
[29] Giannopoulos AA, Mitsouras D, Yoo SJ, Liu PP, Chatzizisis YS, Rybicki FJ. Applications of 3D printing in cardiovascular diseases. Nat Rev Cardiol 2016;13: 701—18.